Vol.11, No.3, October 2025

Available online at: http://e-journal.unair.ac.id/index.php/JISEBI

# **Diabetic Retinopathy Fundus Image Classification Using Self-Organizing Maps**

Yulius Denny Prabowo 1)\* D, B. Yudi Dwiandiyanta 2), Martinus Maslim 3) , Andrea Corradini 4)

<sup>1)</sup> Computer Science Department, BINUS Online Learning, Bina Nusantara University, Jakarta, Indonesia <sup>1)</sup>yulius.denny@binus.ac.id

<sup>2)3)</sup> Informatics Department, Faculty of Industrial Technology, Universitas Atma Jaya Yogyakarta, Daerah Istimewa Yogyakarta, Indonesia

<sup>2)</sup>yudi.dwiandiyanta@uajy.ac.id, <sup>3)</sup>martinus.maslim@uajy.ac.id

<sup>4)</sup> Digital Business & Software Engineering, MCI 6020 Innsbruck, Austria

#### Abstract

**Background:** Diabetic retinopathy (DR) is a condition that impairs the blood vessels in the retina, resulting in vision loss ranging from temporary to permanent blindness. It commonly affects individuals diagnosed with diabetes mellitus (DM). Fundoscopy is a technique used to identify DR by examining the fundus of the eye during an eye examination. This process is time-consuming and can be expensive.

Objective: This study aimed to examine the identification of DR using digital image processing methods.

**Methods:** The self-organizing map (SOM) artificial neural network was employed. Diabetic retinopathy will be categorized according to its severity, including normal, mild, moderate, or severe. This classification considers the quantity of exudates and microaneurysms and the blood vessel structure in the fundus image. The dataset used in this investigation comprised 1000 fundus images acquired from the MESSIDOR ophthalmology database.

**Results:** The findings indicate that the SOM approach achieves a training accuracy of 72% and a testing accuracy of 62%. **Conclusion:** The DR severity classification system can effectively extract DR-related features by segmenting exudates, blood vessels, and microaneurysms from funduscopic images during training, testing, and evaluation.

Keywords: Diabetic Retinopathy, Self-Organizing Map, Fundus Image Classification, Digital Image Processing

Article history: Received 14 April 2025, first decision 27 May 2025, accepted 10 September 2025, available online 28 October 2025

# I. INTRODUCTION

Hyperglycemia occurs when the blood glucose level is higher than usual. It affects people with diabetes mellitus (DM), but it can also develop in nondiabetics. Patients with diabetes cannot metabolize glucose because either their pancreas does not produce enough insulin, which is essential to control glucose levels, or their body cannot effectively use the insulin it produces. Hyperglycemia can lead to several complications, such as skin problems and infections, kidney damage, eye diseases, cardiovascular diseases, and nerve damage, over time [1]. Diabetic retinopathy (DR) is a severe eye condition caused by diabetes mellitus, leading to potential blindness if left undiagnosed and untreated. Fundus imaging is a standard noninvasive method used for the screening of DR. ML and deep learning techniques have enhanced DR detection, classification accuracy, and efficiency.

In 2021, Indonesia ranked fifth among countries with the highest prevalence of DM, with 19.5 million individuals affected [2]. DR is higher in older individuals with DM due to their advanced age and longer duration of diabetes [3]. DR can be classified into two main categories: NPDR and PDR. NPDR is the deterioration of the retina's blood vessels. Fluid and blood can sometimes flow into the retina in specific instances. Blood vessels appear dilated, with uneven vessel margins. Proliferative diabetic retinopathy (PDR) can develop from NPDR-type diabetic retinopathy when the damage to blood vessels in the retina increases. The PDR type results in vascular damage, forming aberrant blood vessel segments in the retina [4]. This disrupts the regular circulation of fluid in the eye. The ocular globe will undergo elevated IOP. In 2020, the number of adults worldwide with DR was estimated to be approximately 103 million, projected to increase to approximately—160 million by 2045 [5]. An early study showed that of 1785 patients

<sup>4)</sup>andrea.corradini@mci.edu

<sup>\*</sup> Corresponding author

in Indonesia who had T2DM, a significant 42% developed several complications [6]. Of the total number of people with DR, 8.3% have NPD Retinopathy.

Various classification algorithms have been explored, including CNNs, SVMs, and ensemble methods [7], [8], [9], [10]. A specific study on SOM for DR classification involved converting fundus images to grayscale, applying edge detection and morphological operations, and then using SOM for classification. This method achieved 93.7% accuracy in identifying different eye conditions, including DR [11]. Fundoscopy is one method for identifying individuals with DR. Funduscopy is a diagnostic procedure that involves the inspection of the fundus of the eye, which includes the structures, such as the retina, located behind and inside the eye. This was examined using an ophthalmoscope or Fundus photography [4]. However, even after acquiring the fundus image by fundoscopy, the specialists would still need extra time to determine DR. Early detection of DR is crucial in preventing its progression to severe stages.

While deep learning methodologies have attained superior performance in DR detection, they incur substantial expenses regarding computational power and labeled data, rendering their implementation in low-resource settings challenging [7], [8], [9]. Furthermore, they possess the black-box problem, rendering clinical interpretation challenging [10], [12]. This creates a need for a simpler and more understandable method, such as self-organizing maps (SOM), which is still rarely used in classification tasks that reduce data dimensions, despite its potential for unsupervised learning and visual interpretation. SOM, introduced by [13], is an unsupervised neural network that projects high-dimensional data onto a lower-dimensional space while preserving topological relationships among the input data [13]. This makes it highly suitable for analyzing complex biomedical images such as fundus photographs, especially in low-resource settings where interpretability and computational efficiency are crucial [14]. SOM also offers visual insights into clustering behavior, distinguishing it from black-box models.

Some prior research supports its applicability, such as [11], which demonstrated the effectiveness of SOM in detecting multiple types of eye disease, achieving 93.7% accuracy. Similarly, [15] used SOM to analyze macular morphological patterns in diabetic retinopathy, and [16] successfully applied SOM with k-means clustering for retinal vessel segmentation. These examples reinforce the rationale for applying SOM in this study, given its strengths in unsupervised classification, dimensionality reduction, and clinical interpretability.

This research reports on developing a model that can detect and categorize the degree of DR severity using fundus images. The objective is to assist specialists in quickly identifying DR and implementing suitable medical interventions. This study categorized the DR levels into four distinct levels: normal mild moderate, and severe. The severity of DR is based on the number of exudates and microaneurysms and the condition of the blood vessels. Self-organizing maps (SOM) can help classify medical images, including fundus images, for detecting drowsiness (DR). SOMs were employed to analyze fundus image data acquired from a fusion of MESSIDOR ophthalmology databases [17].

The primary contributions of the current paper are as follows: (1) We present a hybrid model that utilizes morphological preprocessing, CLAHE contrast enhancement, and SOM-based classification for the detection of DR stages; (2) We demonstrate that this streamlined model yields results comparable to more complex deep learning methods, particularly in identifying the early stages of DR; (3) We demonstrate that our model is interpretable, scalable to extensive datasets, and suitable for deployment in resource-limited clinical settings, thereby facilitating the democratization of retinal screening technology.

## II. LITERATURE REVIEW

Extensive research and development have been conducted on the DR categorization. Several studies, such as the one reported in [18], categorize DR severity into four distinct classes: normal, NPDR, PDR, and macular edema. This study utilized the statistical characteristics of patient fundus images acquired through a feature extraction technique, specifically by comparing two methods: 3D-GLCM extraction and 3D-GLCM projection. Once feature extraction is complete, the subsequent phase involves training these features using a backpropagation ANN. The research findings demonstrate that the developed system can perform classification with 100% sensitivity, 91% specificity, and 95.83% accuracy. In another study [19], 250 test data were used to evaluate the accuracy of a particular extraction and classification method based on LVM. The results show an accuracy rate of 93.33% and a computing time of 0.7195 s. The accuracy of the classification results is affected by various parameters, such as image resizing size, orientation angle, and spacing between pixels.

An additional recent study on DR identification using the Kirsch edge detection and watershed transformation technique was conducted in [20]. The watershed transformation is a segmentation method designed explicitly for grayscale images. This algorithm was selected based on its superior performance when applied to input images with distinct edges. Since the fundus images used in this study are primarily gradient images, the watershed transformation can generate segmentations that appear as closed contours representing the segmented regions. This study categorized

DR into three classes: mild, moderate, and severe. Based on the results, using the watershed transformation algorithm seems useful in facilitating human detection of DR due to its ability to identify anomalies in fundus pictures that are imperceptible to the unaided eye.

A recent study [21] explains that the classification of DR severity in fundus images involves multiple stages of image preprocessing and feature enhancement. Their method includes contrast adjustment, preservation of vessel structure, and extraction of attention-based features using a hybrid architecture that combines a residual attention network and a vision transformer. This approach enables more accurate retinal lesion discrimination by enhancing the visibility of pathological features critical to DR diagnosis. DR severity was classified into multiple stages, ranging from no DR to proliferative DR. The proposed model outperformed conventional CNN-based methods and achieved a classification accuracy of up to 96.08%, demonstrating the effectiveness of combining global and local attention in improving DR classification performance.

Another study [22] proposed a microaneurysm detection framework using mathematical morphology for fundus image enhancement, red structure extraction (e.g., blood vessels), and true microaneurysm candidate selection via feature extraction. Their approach achieved a sensitivity, specificity, and accuracy of 89.22%, 91%, and 92%, respectively, on the DiaretDB1 dataset and 83% sensitivity with 82% specificity on the eophtha dataset. A study on microaneurysm identification using the Raspberry Pi and the OpenCV library was conducted in [23]. The test data consisted of 55 fundus photographs obtained from the Messidor digital database [17]. The authors of that study contend that employing the Raspberry Pi can yield superior computational performance compared to software that relies on simulation. A real-time camera equipped with a Raspberry Pi controller board can capture color images. This also allows for the inclusion of additional factors and features that can enhance DR identification.

# III. METHODS

This section explains the methodology employed in this study. Figure 1 schematically illustrates the processing steps undertaken in this study. The following subsections provide a comprehensive explanation of the steps that comprise the entire process. Figure 1 shows the research methodology, starting with data collection and preprocessing, training and testing, and evaluation.

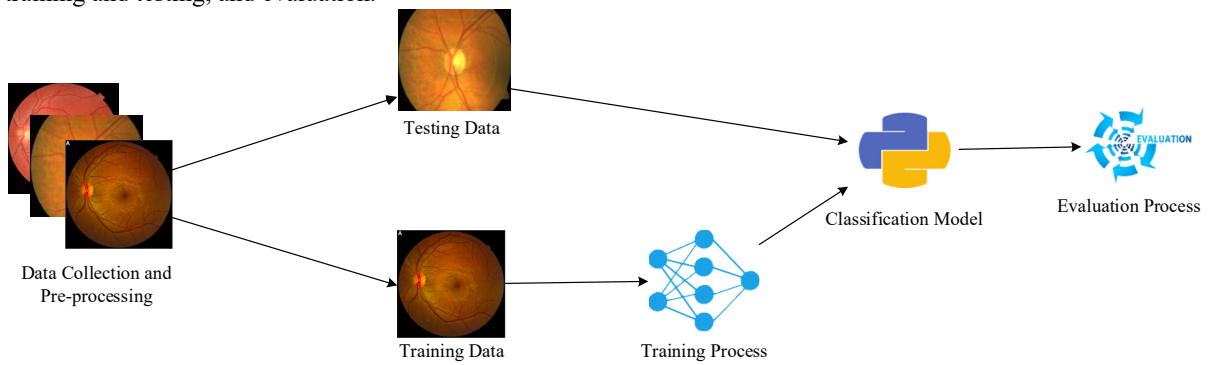


Fig. 1 Research Methodology

## A. Data Collection

We gathered 1000 fundus image datasets from the MESSIDOR ophthalmology database [17]. The dataset was then divided into four distinct data chunks, each representing a different category based on the severity levels of DR. Each category is characterized by the quantity of observed exudates and microaneurysms and the blood vessel morphology. The following severity levels of DR were considered: normal mild moderate, and severe. Table 1 displays the data for each class in pictures, while Table 2 shows the features of each category. Table 1 illustrates the frequency of fundus images based on the severity of DR. The data were categorized into four classifications: normal, mild, moderate, and severe. Specifically, 546 photos were classified as normal, 153 as mild, 247 as moderate, and 254 as severe.

TABLE 1
THE NUMBER OF PICTURES CATEGORIZED BY SEVERITY LEVEL

| Severity | Number of Images |
|----------|------------------|
| Normal   | 546              |
| Mild     | 153              |
| Moderate | 247              |
| Severe   | 254              |

Table 2 presents a detailed description of the severity levels of DR based on its clinical characteristics as demonstrated in fundus pictures. The normal group is defined by the lack of DR indicators, including a healthy ocular condition and the absence of microaneurysms and hemorrhages. The mild category is characterized by microaneurysms within a restricted range without spot or blot hemorrhages. No discernible alterations are seen in the blood vessels; however, cotton wool spots (CWS) or soft exudates may occasionally be observed. The moderate stage is characterized by microaneurysms of 5–15 m, typically accompanied by no more than five spot and blot hemorrhages. IRMA may also manifest at this stage, indicating beading or irregularities in venous blood vessels, with either soft or hard exudates. In the Severe stage, numerous microaneurysms ( $\mu$ A), exceeding 15, are present in the eye, spread uniformly throughout all fundus quadrants. This phase includes several blot hemorrhages and venous beading in two or more quadrants, together with potential intraretinal microvascular abnormalities (IRMA) in one quadrant, indicating significant vascular damage and advanced DR stages.

TABLE 2
CATEGORIZATION OF THE SEVERITY LEVELS OF DIABETIC RETINOPATHY

| Severity | Description  |
|----------|--|
| Normal   | Good eye health and no signs of Diabetic Retinopathy were seen.  |
| Mild     | Microaneurysms were identified with a range of $0 < \mu A \le 5$ , No spot or spot hemorrhages (dot and blot hemorrhages) were |
|          | found, and the blood vessels appear normal. Cotton wool spots (CWL) or soft exudates may be observed (optional).               |
| Moderate | A microaneurysm is discovered when its size falls within the 5 to 15 μA range. A total of 0 to 5 spots and spot hemorrhages,   |
|          | also known as dot and blot hemorrhages, were identified. Intraretinal Microvascular irregularities (IrMA) result in venous     |
|          | beading or irregularities in blood vessels. Soft exudates and hard exudates identified (optional)                              |
| Severe   | Numerous microaneurysms (µA) were discovered, with a minimum of 15 microaneurysms being present. Multiple point                |
|          | hemorrhages are evenly distributed in all four quadrants of the fundus, with a minimum count of H>= 5. Venous beading occurs   |
|          | when there is an aberrant spread of IrMA to the fundus quadrant or irregularities in the blood vessels.                        |

After collecting the data, a pre-processing step was performed to ensure the consistency of the dataset and filter out nonrelevant information. The initial pre-processing steps involved image resizing. Fundus images must be resized due to the variability in the dimensions of the image dataset. We resized the input images to dimensions of 80x80 pixels to provide uniformity and mitigate the computing process. Furthermore, the image color space was converted to the green channel. The green channel of the RGB color space offers superior and more discernible contrast among blood vessels, exudates, and microaneurysms than the red and blue channels.

TABLE 3
STAGES OF PREPROCESSING IN FUNDUS IMAGES
Preprocessing Process

Resize Image

Green Channel Extraction

CLAHE Algorithm Implementation

Optic Disc Elimination

After extracting the green channel from an image, we applied contrast enhancement using the CLAHE algorithm. The CLAHE algorithm improves the contrast in the localized regions of the image referred to as tiles. The contrast of each tile was carefully boosted to provide a uniform histogram. The augmented photos were amalgamated using

interpolation. Optic discs and exudates exhibit analogous colors in fundus pictures but differ in form and size. Consequently, optic discs were identified in the preprocessing phase via the Hough Circle transform by locating the largest and most luminous circle inside the fundus image region. This step aims to improve the quality of image features and remove optical discs. All dataset components, including the training and testing data, were preprocessed. An example of the visual representation of one fundus picture as it undergoes several preprocessing phases is shown in Table 3.

## B. Data Preprocessing

After collecting the data, we performed a pre-processing step to ensure the consistency of the dataset and filter out non-relevant information from the dataset. The initial pre-processing steps involved resizing the image. Resizing fundus images is necessary due to the variability in the dimensions of the image dataset. We resized the input images to dimensions of 80x80 pixels to provide uniformity and mitigate the computing process. Further, we converted the image color space to the green channel. The green channel of the RGB color space offers superior and more discernible contrast among blood vessels, exudates, and microaneurysms than the red and blue channels.

After extracting the green channel from an image, we applied contrast enhancement using the Contrast Limited Adaptive Histogram Equalization (CLAHE) algorithm. The CLAHE algorithm improves contrast in localized regions of the image referred to as tiles. Each tile's contrast was carefully boosted to provide a uniform histogram. The augmented photos were amalgamated by interpolation. Optic discs and exudates exhibit analogous colors in fundus pictures but differ in form and size. Consequently, optic discs were identified in the preprocessing phase via the Hough Circle transform by locating the largest and most luminous circle inside the fundus image region. This step aims to improve the quality of image features and remove optical discs. The preprocessing step was performed on all dataset components, including the training and testing data. Table 3 shows an example of the visual representation of one fundus picture as it undergoes several preprocessing phases.

## C. Image Segmentation

The next step consisted of a segmentation task. Three segmentation processes were conducted: exudate, microaneurysm, and blood vessel segmentation. All segmentations were performed on the preprocessed data. The method used to extract the exudate feature from the image involved the dilation morphological transformation, which was applied to augment pixels at the object's periphery, enhancing the object's boundaries' visibility. A binary threshold was used to convert the image pixels from grayscale to a binary format for enhanced analysis. Upon obtaining the picture segmentation, a median filter was employed on the resulting image to reduce noise.

The segmentation approach employed to extract the microaneurysm feature from preprocessed images involved gamma compensation through color mapping to an array. After obtaining the array via color mapping, two morphological operations were applied: top-hat transform with a 9x9 kernel and opening morphological operator with a 7x7 kernel. Eventually, a threshold was used to convert the image into a binary format.

TABLE 4
DIABETIC RETINOPATHY FEATURES SEGMENTATION RESULTS

Segmentation Exudates Blood Vessels Microaneurysms

Result

The segmentation approach utilized to extract blood vessel characteristics from the preprocessed image involved the application of alternate sequential filtering (ASF), which consists of three closure and opening morphological transformation procedures using varying kernel sizes. The ASF results were deducted from the CLAHE results during preprocessing. Additionally, the resultant image from the subtraction was processed once through the thresholding and erosion procedures. The final segmentation method relied on the findContours function in OpenCV, which was used to identify intricate blood vessel architecture in fundus pictures.

Then, the three segmentation results of the DR features were integrated. The aggregated image segmentation results are used as input in the training, testing, and classification procedures. Table 4 displays images obtained from the segmentation of the exudates, blood vessels, and microaneurysms.

## D. Training Process

The SOM method was adopted to generate our classification model. The SOM was selected for its proven efficacy in unsupervised pattern categorization and dimensionality reduction, especially with high-dimensional medical imaging data. high-dimensional, complex inputs onto a lower-dimensional lattice with a topological neighborhood structure, rendering the resultant representation interpretable and suitable for clustering applications [13]. Some research indicates that self-organizing maps (SOMs) have been effectively utilized in medical imaging and feature organization, with retinal vascular segmentation being one such application [15], [16]. Recently, self-organizing maps (SOMs) were used to cluster fundus images in a diabetic retinopathy study, demonstrating that this lightweight and unsupervised approach can be an efficient and interpretable alternative to DL models [16]. The SOM structure comprises nodes associated with a specific weight as a vector representing the node's position within the dataset space. SOM training involves adjusting the weights based on the input data. The goal of training is to reduce the distance (different metrics can be used) between the weights and any given input without modifying the node topology. When used in classification mode, the idea is to activate the node closer to the input. In other words, the node that responds to a specific input has the most similarity to all inputs that follow specific input patterns [24]. Different methods, such as k-means, hierarchical clustering, and graph-based approaches, are used to cluster the neurons in SOM, each with its advantages and considerations [25], [26], [27], [28]. This study uses the SOM algorithm to partition the data into k clusters [29]. The sequential process of how the SOM network performs on the training data is as follows: The initial values of the neural network node weight vector (wij) are set by randomly selecting a value or using equation 1.

$$w_{ij} = \frac{\min(x_i) + \max(x_i)}{2} \qquad (1)$$

The weight wij represents the strength of the connection between the j-th input variable and the i-th neuron. min(xi) represents the smallest value of the ith input variable, whereas max(x<sub>i</sub>) represents the most significant value of the ith input variable. Subsequently, we set the neighbor width (neighborhood function)  $\theta$  to its initial value. The next step is to set the learning rate parameter α to its initial value. Then, iterate through each input vector x and perform the following steps. The distance D(j) for each neuron j, which represents the distance between the input data and the neuron in the map, as defined by equation 2.

$$D(j) = \sum_{i}^{n} \left( w_{ij} - x_i \right)^2 \quad (2)$$

 $D(j) = \sum_{i=1}^{n} (w_{ij} - x_i)^2 \quad (2)$  The second step determines the lowest distance, D(j), which determines the winning neuron. Consequently, the victorious neuron is modified to resemble the input variable x and its adjacent neurons. The weights assigned to the winning neuron j and its adjacent neurons were assessed, as shown in equation 3.

$$w_{ij}(next) = w_{ij}(prev) + \theta * \alpha [x_i - w_{ij}(prev)]$$
(3)

The winning neuron will receive a new weight, denoted as wij(next), which will substitute the prior weight, w<sub>ij</sub>(previous), or the former weight.

The next sequential process of how the SOM network performs is to revise the learning rate  $\alpha$  using equation 4.  $\alpha(t) = \alpha_i \left(1 - \frac{t}{t_{max}}\right) \tag{4}$ 

$$\alpha(t) = \alpha_i \left(1 - \frac{t}{t_{max}}\right) \quad (4)$$

The value of the learning rate  $\alpha$  will drop as the iteration progresses. Simultaneously, decrease the breadth of the neighboring region (neighborhood function) sθ. The last step is to repeat step 4 until the map reaches convergence, which is indicated by a lack of substantial weight changes or until the predetermined training cycle value has been attained. The weight at the end of the map iteration is used as the categorization model.

TABLE 5 THE NUMBER OF TRAINING AND TESTING DATA

| Severity — | The Number of Images |         |  |
|------------|----------------------|---------|--|
|            | Training             | Testing |  |
| Normal     | 201                  | 95      |  |
| Mild       | 123                  | 66      |  |
| Moderate   | 194                  | 85      |  |
| Severe     | 190                  | 46      |  |
| Total      | 708                  | 292     |  |

The training and testing sets were manually divided based on the number of images in each DR severity group. Table 5 shows the specifics of partitioning the image dataset into training and testing sets. Table 5 illustrates the distribution of training and testing data for the severity of DR. The data were categorized into four severity categories: Normal, Mild, Moderate, and Severe. The training set included 708 photos, comprising 201 Normal, 123 Mild, 194 Moderate, and 190 Severe images. The testing set included 292 photos, including 95 normal, 66 mild, 85 moderate,

and 46 severe images. Two methodological modifications were implemented to improve the classification performance. To enhance SOM training, we preprocessed the pertinent retinal structures using CLAHE-based techniques, followed by morphological operations to improve the quality of the features. Second, we adjusted the parameters of the self-organizing map (e.g., map size and learning rate) based on validation using labeled subsets of the MESSIDOR database. These improvements enable the SOM to establish more precise boundaries between classes and enhance precision in determining the severity of DR.

#### IV. RESULTS

This section analyzes the outcomes obtained from training and testing the classification model and discusses several test conditions.

## A. Training Model

The fundus image model was trained on the PyCharm Community Edition using the NVIDIA GeForce 920MX graphics card. The training duration ranges from 45 to 60 minutes. The model was evaluated by adjusting the SOM parameters. The setting for the neuron size is set to 20x20. The sigma/neighbor radius parameters are assessed using values 4, 5, and 6. The learning rate parameters are estimated using values ranging from 0.1 to 1 with different increments. Finally, the number of iterations parameter is assessed using the 2000, 5000, and 6000 values. The accuracy of the model testing is determined by comparing the classification results and the outcomes of grouping DR severity from the dataset or ground truth. The evaluation process revealed that the highest accuracy was achieved in SOM training and testing using neuron size parameters of 20x20, a sigma value of 5, a learning rate of 0.5, and 5000 iterations. The training accuracy reached 72%. Table 6 displays the highest accuracy values obtained during model training and testing. Table 7 shows the training classification report, which shows 72% accuracy. Table 8 presents the test classification report, which shows 62% accuracy. Tables 7 and 8 denote class labels using the numbers 0-3, with 0 signifying normal, 1 indicating mild, 2 representing moderate, and 3 denoting severe.

TABLE 6 Evaluation of Diabetic Retinopathy Severity Model

|             | EVALUATION OF DIABETIC RETINOPATHY SEVERITY MODEL |               |                  |                   |                  |
|-------------|---|---------------|------------------|-------------------|------------------|
| -           | SOM Parameter                                     |               | Testing Accuracy |                   |                  |
| Neuron Size | Sigma   | Learning Rate | Iteration        | Training Accuracy | resting Accuracy |
| 20 x 20     | 4   | 0.5           | 2000             | 65 %              | 51 %             |
| 20 x 20     | 4   | 0.5           | 5000             | 70 %              | 50 %             |
| 20 x 20     | 4   | 0.9           | 5000             | 68 %              | 59 %             |
| 20 x 20     | 4   | 1.0           | 5000             | 59 %              | 55 %             |
| 20 x 20     | 5   | 0.5           | 2000             | 63 %              | 54 %             |
| 20 x 20     | 5   | 0.5           | 5000             | 72 %              | 62 %             |
| 20 x 20     | 6   | 0.6           | 2000             | 54 %              | 51 %             |
| 20 x 20     | 6   | 0.5           | 5000             | 57 %              | 56 %             |
| 20 x 20     | 5   | 0.5           | 6000             | 71 %              | 50 %             |
| 20 x 20     | 5   | 0.6           | 6000             | 69 %              | 54 %             |

TABLE 7

|              | TRAINING CLAS | SSIFICATION I | REPORT   |         |
|--------------|---------------|---------------|----------|---------|
| Severity     | Precision     | Recall        | F1-Score | Support |
| Normal       | 0.74          | 0.71          | 0.72     | 201     |
| Mild         | 0.80          | 0.67          | 0.73     | 123     |
| Moderate     | 0.71          | 0.70          | 0.70     | 194     |
| Severe       | 0.67          | 0.77          | 0.72     | 190     |
| accuracy     |               |               | 0.72     | 708     |
| macro avg    | 0.73          | 0.71          | 0.72     | 708     |
| weighted avg | 0.72          | 0.72          | 0.72     | 708     |

TABLE 8

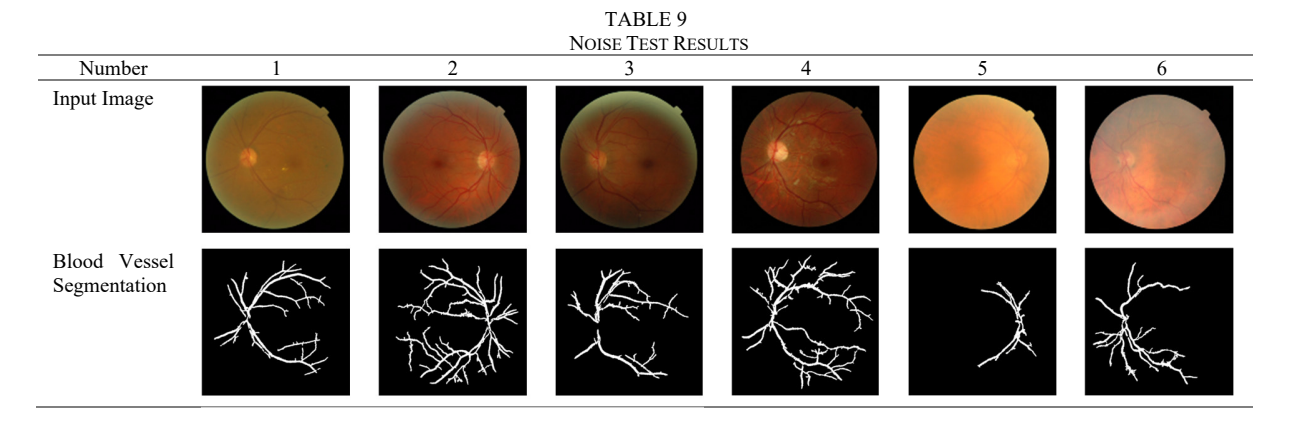
|              | TESTING CLASSIFICATION REPORT |        |          |         |
|--------------|-------------------------------|--------|----------|---------|
| Severity     | Precision                     | Recall | F1-Score | Support |
| Normal       | 0.59                          | 0.56   | 0.59     | 95      |
| Mild         | 0.89                          | 0.59   | 0.72     | 66      |
| Moderate     | 0.57                          | 0.53   | 0.58     | 85      |
| Severe       | 0.47                          | 0.61   | 0.56     | 46      |
| accuracy     |                               |        | 0.62     | 292     |
| macro avg    | 0.63                          | 0.57   | 0.62     | 292     |
| weighted avg | 0.63                          | 0.57   | 0.61     | 292     |

#### B. Test Conditions

This section presents the test results for multiple variations of the input image conditions.

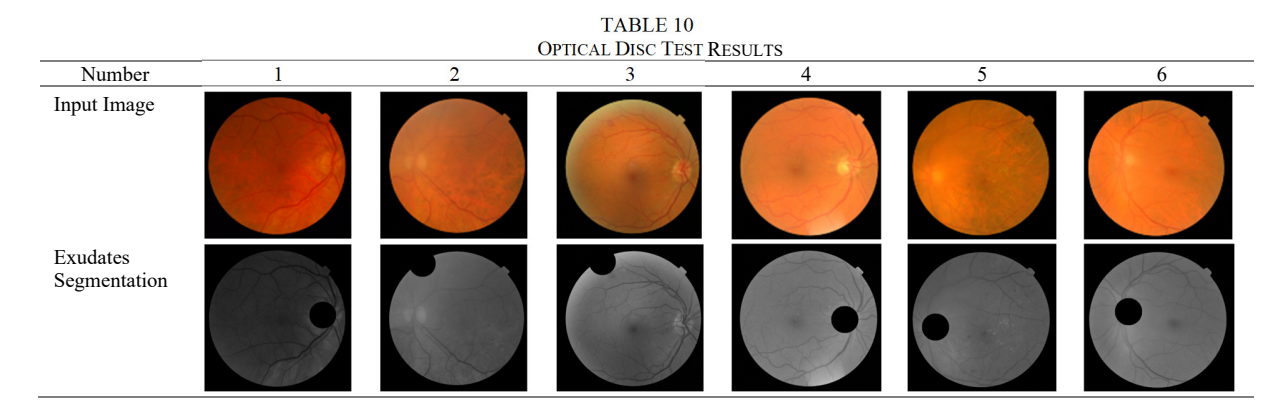
## 1) Input image containing noise

Noise refers to the random variation in the brightness or color data of an image. Noise refers to the reduction in an image's signal due to external factors. Images with noise exhibit a direct relationship between an area's brightness and the level of the noise present in that area. Noise may arise in funduscopic images when using a fundus camera due to inadequate lighting, lens magnification, and improper image capture angles. The system underwent testing by segmenting blood vessel features due to its larger segmentation area scale compared with exudates or microaneurysms. This choice was made to ensure that the impact of noise would be easily discernible. Table 9 presents the noise test results for the blood vessels feature, which includes 6 test photos displaying both noise and the corresponding blood vessel segmentation results.



#### 2) The input image does not contain a distinct optical disc object

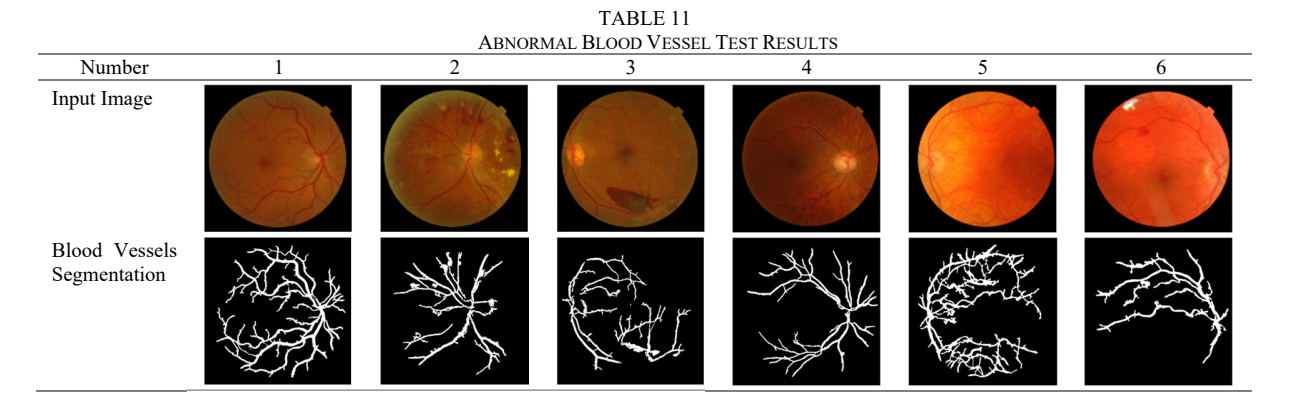
Incorrect fundoscopy can lead to indistinct or absent depiction of specific characteristics in the image. The optic disc/retina of the eye might be affected in this particular region. An indistinct region of the optic disc/retina can impede the segmentation process of exudates because the optic disc area must be excluded during this procedure. We hypothesize that the system may inaccurately identify the optic disc area when it is either not visible or absent in the input image. Table 10 presents the test results for optical disc areas that are not easily distinguishable in the exudate feature. This includes six test photos containing indistinct optical disc objects.



## 3) Abnormal morphology of blood vessels

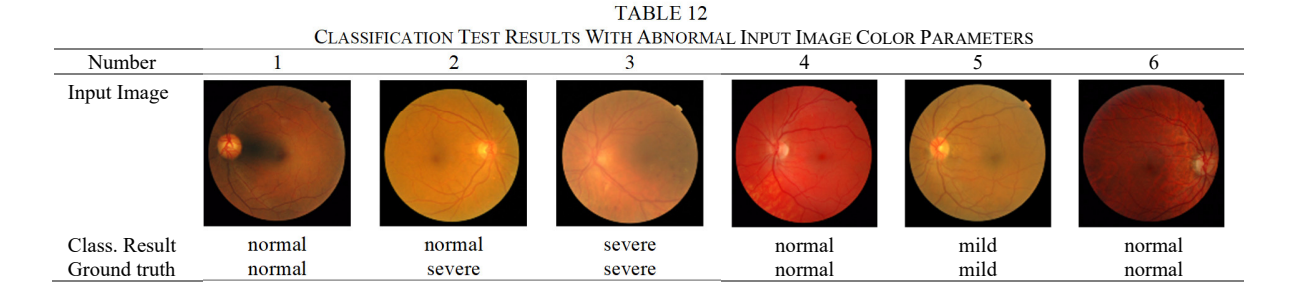
Multiple input images exhibit funduscopy with intricate blood vessel structures resulting from blood vessel irregular branching or broadening. The frequency of these occurrences seems to increase in correlation with DR severity. Under specific circumstances, the anatomy of blood vessels can appear more straightforward due to the varying angles at which fundoscopic images are captured. When certain sections of the vessels get obstructed by other elements, such as exudates or microaneurysms, separating the branching pathways, an additional issue with the arrangement of blood arteries arises. This test evaluated the ability of the system to accurately separate blood vascular characteristics with a

complicated and aberrant structure. Table 11 presents the findings of the abnormal blood vessel structure segmentation test, which comprises six images of abnormal blood vessel structures.



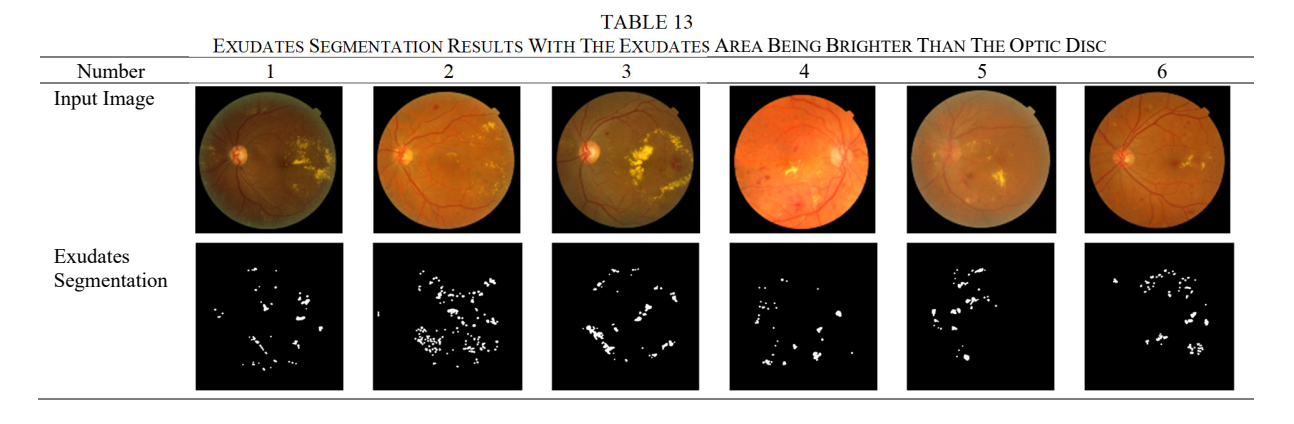
## 4) Abnormal color parameters of the input image

Variations in the color code of the funduscopy input image result from the lighting capacity and type of fundus camera used during the image-capturing procedure. Clusters of images within this collection of funduscopic photos exhibit anomalous color coding. This examination assesses the capacity of the system to classify funduscopic images based on aberrant color codes. Table 12 displays the test results, which show the classification test results with abnormal input image color parameters.



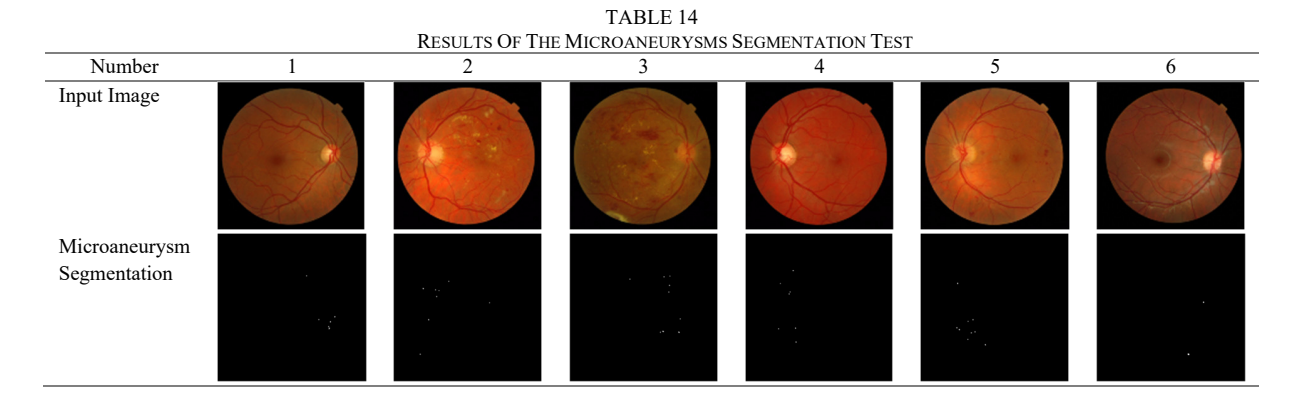
# 5) A region in the fundus has a higher level of brightness than the area around the optic disc.

The exudate characteristics are occasionally the most prominent in fundoscopic images. This can disrupt the segmentation process of exudates because this characteristic shares a similar color coding with the optic disc, causing the optic disc area to be mistakenly identified as an exudate feature. This test assesses the ability of the system to handle segmentation with exudate patches that have a higher brightness than the optic disc. Table 13 presents the test results for the input image, where the fundus area is brighter than the optic disc area.



### 6) The microaneurysm segmentation failed due to the input image scaling

As part of the preprocessing for diabetic retinopathy feature segmentation, the image is resized to dimensions of 80x80 pixels to decrease the computational burden. However, if the image dimensions are too small during the segmentation phase, the system will fail to distinguish microaneurysms, which are the smallest among the other attributes. The author's technique involves segmenting these characteristics using an input image of the exact dimensions. Table 14 displays the outcomes of the microaneurysm segmentation testing.



## V. DISCUSSION

Table 7 shows the classification test report of each class. The evaluation of the SOM model on the training data indicates that the trained model applies to the classification of DR severity levels, achieving optimal and stable top classification results. The precision, recall, and F1-score for the Normal class (label 0) were 0.74, 0.71, and 0.72, respectively, demonstrating the effective differentiation of healthy retinal images. The Mild DR class (label 1) exhibited the best precision of 0.80, suggesting that predictions of mild cases are likely accurate; however, the recall was lower at 0.67, indicating that some mild cases were misclassified as other levels. The moderate DR class (label 2) exhibited balanced precision and recall, with both metrics at 0.70. However, there was a minor disparity in the difficulty of data separation, rendering classification more challenging. The elevated recall (0.77) for the Severe DR class (label 3) suggests that the model is reasonably adept at identifying advanced-stage DR cases; however, the accuracy is only 0.67, indicating a propensity for false positives in related categories. The SOM model achieves a training accuracy of 72%, with both macro and weighted average F1-scores of 0.72, indicating a clear and fairly consistent classification of all DR levels. The results suggest that the model has potential as an accessible and cost-effective instrument for detecting DR, particularly in resource-limited settings.

Table 8 presents the testing classification report of each class. The evaluation of the SOM model within the test range, comprising 292 fundus pictures, indicates moderate classifier performance across various DR severity phases. For the Normal class (label 0), the model exhibited an accuracy of 0.59 and a recall of 0.56, resulting in a suboptimal F1-score of 0.59, indicating that the model's ability to distinguish healthy retinas is inconsistent. The model performed optimally on the Mild DR class (label 1), achieving a notable precision of 0.89 and an F1-score of 0.72; however, the recall decreased to 0.59. Although the model exhibits considerable confidence in classifying a case as mild DR, it still fails to identify many mild instances. The model exhibited satisfactory performance for the Moderate DR class (label 2), albeit with marginally lower precision and recall values of 0.57 and 0.53, respectively, resulting in an F1-score of 0.58. The most challenging category was Severe DR (label 3), with the model exhibiting a precision of 0.47 and a recall of 0.61, indicating that other instances are more frequently misclassified as severe, whereas severe cases are correctly identified. The SOM model achieved a test accuracy of 62%, with a macro-average F1-score of 0.62 and a weighted average F1-score of 0.61. The results suggest that while the SOM model shows promise in accurately detecting mild DR, further refinement is necessary to improve its recall and provide consistent stability across all DR severity levels.

Table 9 shows that the system accurately segmented blood vessel characteristics in the first, second, third, and sixth test images, even when the input images contained noise. When input photos are used, noise levels within acceptable limits do not impede the blood vessel segmentation procedure. In the fourth test image, the system failed to detect the blood vessels to the right of the optic disc due to their excessive brightness produced by their proximity to exudate characteristics. The ability of the system to segment the blood vessels of the input image is hindered when the image has excessive and artificial noise, as seen in the fifth image, which obscures the crucial aspects of DR.

The system successfully identified and removed the optic disc in the first, fourth, fifth, and sixth test images (Table 10). The technology can effectively address areas of the optic disc that exhibit blurriness or noise. Nevertheless, the method failed to identify and remove the optic discs that were not distinctly evident in the second and third test images. This is due to a lack of good visibility of the optic disc area, leading to reduced brightness in the optic disc's surrounding area. Applying this criterion, the algorithm will identify the brightest circle within a given location. The illumination intensity in the optic disc region is often diminished, causing the system to detect additional circular shapes that are not optical disc objects. The algorithm identified an area in the top left portion of the fundoscopy that exhibited more illumination than the optic disc in the second and third test images.

The result in Table 11 explains that the system successfully segmented blood vessel features with abnormal structures in all six test photos, including complicated abnormal branches in the first, second, and fifth images and fundamental abnormalities in the fourth and sixth images. The system remains unaffected by a hemorrhage feature in the bottom center of the third test image, even if it partially obscures the feature of the blood vessel.

Table 12 shows that the method accurately classifies the severity of DR on the first, third, fourth, fifth, and sixth test photos, matching the ground truth class. However, the system failed to accurately categorize the second test image's fundus image as severe. The proximity of the color parameters of the input image to the color of the exudates causes this phenomenon. The second image exhibits exudates as the primary characteristic, leading to the severity classification as severe. The second image is categorized as having normal severity due to the inability of the system to detect exudates.

Table 13 shows that the method accurately segmented the exudate features in the second and sixth test images. Although most exudate features in the first and third test images could be successfully segmented, the exudates on the right side of the fundoscope were not detected. The exudates are positioned at the periphery of the fundoscopy, near the interference caused by inadequate image acquisition. Exudates were detected in the optic disc area of the fourth and fifth test photos. This is due to the elimination process of the optic disc, which identifies the location of the exudate with the highest brightness level.

The results in Table 14 explain that the algorithm successfully identified and separated microaneurysm features accurately and precisely in all six test images. This was achieved when the input image used for segmentation maintained its original size and no shrinking was performed during preprocessing. The system discovered 6, 8, 9, 7, 9, and 2 microaneurysms in the first and sixth test photos, respectively. The input image used is of its original dimensions, and it will undergo resizing during postprocessing to a size of 80x80, as seen in the feature segmentation of other DR.

TABLE 15
COMPARATIVE EVALUATION WITH PREVIOUS STUDIES

| COMPARATIVE EVALUATION WITH FREVIOUS STUDIES |          |
|--|----------|
| Studies                                      | Accuracy |
| This Study*                                  | 62%      |
| [30]   | 43.75%   |
| [31]   | 70.5%    |

We present a performance benchmark in response to the comparative evaluation of our SOM-based model against previous studies on diabetic retinopathy classification (Table 15). The models created by [30] and [31] achieve an accuracy of 43.75% and are tailored to specific working environments with particular devices (e.g., Raspberry Pi). Despite the poor accuracy of our approach, it exhibits robustness in the feature extraction process across many testing situations (e.g., input noise, distorted vascular architecture).

Table 15 compares our study with previous DR classification models, including those by [30] and [31]. Although our approach achieved testing accuracy of only 62%, this result must be interpreted in the context of several contributing factors. First, our dataset was downscaled to 80x80 pixels to reduce the computational complexity of SOM training. Although this downscaling improved the training speed and memory usage, it may have led to the loss of fine-grained features, such as microaneurysms, which are critical for detecting early-stage DR. In contrast, studies by [30] and [31] used larger image dimensions or did not specify size reduction. Our study also focused on three specific retinal features—exudates, blood vessels, and microaneurysms—through detailed segmentation. Although this feature engineering promotes interpretability, other relevant features such as hemorrhages, cotton wool spots, or the optic disc area may have been excluded, potentially affecting classification performance.

The advantages of our method lie in its interpretability, low computational resource requirement, and ease of deployment in low-resource settings—especially important for screening DR in underdeveloped regions. Unlike deep learning models, which are computationally intensive and often require graphics processing units (GPUs), our SOM-based model can be trained and deployed on standard hardware. The limitations of our research include lower

classification accuracy compared to state-of-the-art DL models, performance sensitivity to image size and feature selection, and class imbalance in the dataset.

#### VI. CONCLUSIONS

This study concludes that the DR severity classification system can effectively extract DR-related features by segmenting exudates, blood vessels, and microaneurysms from funduscopic images during training, testing, and evaluation. DR severity could be classified by the system using a SOM. When the neuron size is set to 20, the sigma is set to 5, the learning rate is set to 0.5, and the number of iterations is set to 5000, the system achieves a training accuracy of 72% and a testing accuracy of 62%.

The limited accuracy results from the MESSIDOR database's characteristics, which contains fundus images with an imbalanced class distribution. This is evidenced by the number of pictures in each severity level class: 547 images in the first class (normal severity level), 153 images in the second class (mild severity level), 246 images in the third class (moderate severity level), and 254 images in the fourth class (severe severity level). This can affect the quality of the training and testing process, resulting in suboptimal accuracy levels in both training and testing.

The results demonstrate that the SOM model performs competitively compared with traditional supervised models. It offers the benefits of computing efficiency and interpretability, making it appealing for clinical applications in resource-limited settings. The proposed study's primary contribution is its successful application of an unsupervised method to address a classification problem that is typically excluded from supervised deep learning approaches. Furthermore, the system's elevated sensitivity and specificity in identifying mild types of diabetic retinopathy demonstrate its potential to facilitate early screening, a critical necessity in diabetic eye care.

This study identified some drawbacks. The dataset exhibits an uneven class distribution, with photos of the normal class predominating. This imbalance can diminish categorization accuracy for minority groups, such as moderate and mild. Downscaling photos to 80x80 pixels may result in the loss of minute details, such as microaneurysms. Third, SOM can be used for unsupervised clustering; however, it does not provide probabilistic outputs and may encounter difficulties with ambiguous inputs.

Future considerations will involve integrating SOM with a supervised classifier, such as a support vector machine (SVM) or a deep learning model, to enhance precision. Data augmentation and synthetic data generation techniques, such as SMOTE, may be employed to equilibrate the dataset. Furthermore, attention mechanisms or ensemble methods may be used to improve the identification of early-stage DR. Using a publicly accessible dataset, this study is motivated by the practical needs of nations like Indonesia, where limited resources make traditional screening difficult. The proposed approach can be effectively modified and used in different contexts, thereby enhancing the overall efforts to reduce the incidence of preventable blindness.

**Author Contributions:** *Yulius Denny Prabowo*: Conceptualization, Methodology, Writing - Original Draft, Writing - Review & Editing. *B. Yudi Dwiandiyanta*: Conceptualization, Methodology, Experiment, Writing - Original Draft. *Martinus Maslim*: Conceptualization, Data Curation, Experiment. *Andrea Corradini*: Writing - Review & Editing, Supervision.

All authors have read and agreed to the published version of the manuscript.

Conflicts of Interest: The authors declare no conflict of interest.

**Data Availability:** The dataset that was used in this research can be downloaded at https://www.adcis.net/en/third-party/messidor/

**Informed Consent:** There were no human subjects.

**Institutional Review Board Statement:** Not applicable.

Animal Subjects: There were no animal subjects.

#### ORCID:

Yulius Denny Prabowo: https://orcid.org/0000-0002-5632-3744

B. Yudi Dwiandiyanta: -

Martinus Maslim: https://orcid.org/0000-0001-8437-2992

Andrea Corradini: -

#### REFERENCES

- [1] W. L. Yun and M. R. K. Mookiah, "Detection of diabetic retinopathy using K-means clustering and self-organizing map," *J. Med. Imaging Health Informatics*, vol. 3, no. 4, pp. 575–581, 2013, doi: 10.1166/jmihi.2013.1207.
- [2] Statista Research Department, "Countries with the highest number of diabetics worldwide in 2021." [Online]. Available: <a href="https://www.statista.com/statistics/281082/countries-with-highest-number-of-diabetics/">https://www.statista.com/statistics/281082/countries-with-highest-number-of-diabetics/</a> (accessed Feb. 27, 2025).
- [3] S. D. Solomon et al., "Diabetic Retinopathy: A Position Statement by the American Diabetes Association," *Diabetes Care*, vol. 40, no. 3, pp. 412–418, 2017, doi: 10.2337/dc16-2641.
- [4] N. Tsiknakis *et al.*, "Deep learning for diabetic retinopathy detection and classification based on fundus images: A review," *Computers in Biology and Medicine*, vol. 139, p. 104599, 2021. doi: 10.1016/j.compbiomed.2021.104599.
- [5] Z. L. Teo, Y. C. Tham, M. Yu, M. L. Chee, T. H. Rim, N. Cheung, et al., "Global Prevalence of Diabetic Retinopathy and Projection of Burden through 2045: Systematic Review and Meta-analysis," Ophthalmology, vol. 128, no. 11, pp. 1580–1591, 2021.
- [6] P. Soewondo et al., "Outcomes on control and complications of type 2 diabetic patients in Indonesia," *Med. J. Indones.*, vol. 19, no. 4, pp. 235–244, 2010, doi: 10.13181/mji.v19i4.412.
- [7] O. Deperlioğlu and U. Köse, "Diagnogsis of Diabetic Retinopathy Using Image Processing and Convolutional Neural Network," in Proc. Med. Technol. Nat. Congr. (TIPTEKNO), 2018.
- [8] S. Lu, J. Liu, M. Liu, and Q. Zhao, "A Diabetic Retinopathy Classification Method Based on Improved InceptionV3 Neural Network Model," in Proc. 35th Chin. Control Decis. Conf. (CCDC), 2023.
- [9] V. Basreddy and S. Veerashetty, "Preprocessing, Feature Extraction, and Classification Methodologies on Diabetic Retinopathy Using Fundus Images," in *Proc. Int. Conf. Integr. Intell. Commun. Syst. (ICIICS)*, 2023.
- [10] Y. S. Boral and S. S. Thorat, "Classification of Diabetic Retinopathy Based on Hybrid Neural Network," in Proc. 5th Int. Conf. Comput. Methodol. Commun. (ICCMC), 2021.
- [11] H. Z. R. Eduardo, V. L. Yensi, J. F. M. Escalona, and M. D. Ruiz, "Strategy for the Detection of Types of Eye Diseases Using SOM Neural Network," in *Proc. LACCEI Int. Multi-Conf. Eng. Educ. Technol.*, 2022.
- [12] A. Holzinger, A. Carrington, and H. Müller, "Measuring the quality of explanations: The system causability scale (SCS)," KI Künstliche Intelligenz, vol. 34, no. 2, pp. 193–198, 2020.
- [13] T. Kohonen, Self-Organizing Maps, 3rd ed. Berlin, Germany: Springer, 2001.
- [14] V. Gulshan, L. Peng, M. Coram, M. C. Stumpe, D. Wu, A. Narayanaswamy, *et al.*, "Development and validation of a deep learning algorithm for detection of diabetic retinopathy in retinal fundus photographs," *JAMA*, vol. 316, no. 22, pp. 2402–2410, 2016, doi: 10.1001/jama.2016.17216.
- [15] T. Murakami, N. Ueda-Arakawa, K. Nishijima, T. Akagi, A. Uji, T. Horii, and N. Yoshimura, "Macular morphological patterns in diabetic retinopathy by self-organizing map," *Invest. Ophthalmol. Vis. Sci.*, vol. 53, no. 14, pp. 2851–2851, 2012.
- [16] C. A. Lupaşcu and D. Tegolo, "Automatic unsupervised segmentation of retinal vessels using self-organizing maps and k-means clustering," in *Proc. Int. Meeting on Computational Intelligence Methods for Bioinformatics and Biostatistics (CIBB)*, Berlin, Germany: Springer, 2010, pp. 263–274
- [17] J. Decencière et al., "Feedback on a publicly distributed database: the Messidor database," *Image Anal. Stereol.*, vol. 33, no. 3, pp. 231–234, Aug. 2014, doi: 10.5566/ias.1155.
- [18] C. P. Wilkinson, F. L. Ferris III, R. E. Klein, P. P. Lee, C. D. Agardh, M. Davis, R. D. Dills, A. Kampik, G. Pararajasegaram, and J. T. Verdaguer, "Proposed international clinical diabetic retinopathy and diabetic macular edema disease severity scales," *Ophthalmology*, vol. 110, no. 9, pp. 1677–1682, Sep. 2003, doi: 10.1016/S0161-6420(03)00475-5.
- [19] I. R. Dewi, I. R. Magdalena, and R. Y. Nur, "Klasifikasi Retinopati Diabetik Pada Citra Mata Digital Menggunakan 3D Glcm Dengan Learning Vector Quantization," *J. Inform.*, vol. 6, no. 2, pp. 4186–4193, 2019.
- [20] D. Sn, "Detection of Diabetic Retinopathy Using Kirsch Edge Detection and Watershed Transformation Algorithm," Int. J. Adv. Res. Ideas Innov. Technol., vol. 1, no. 2, 2015.
- [21] Z. Gu, Z. Chen, H. Song, C. Chen, and Y. Yang, "Classification of Diabetic Retinopathy Severity in Fundus Images Using the Vision Transformer and Residual Attention," Computational and Mathematical Methods in Medicine, vol. 2023, Article ID 9831706, 11 pages, 2023.
- [22] S. Joshi and P. T. Karule, "Mathematical morphology for microaneurysm detection in fundus images," *European Journal of Ophthalmology*, vol. 30, no. 5, pp. 1135–1142, Sep. 2020, doi: 10.1177/1120672119843021.
- [23] R. Haldar, S. Aruchamy, A. Chatterjee, and P. Bhattacharjee, "Diabetic Retinopathy Image Enhancement Using Vessel Extraction in Retinal Fundus Images by Programming in Raspberry Pi Controller Board," in *Int. Conf. Interdiscip. Res. Eng. Technol.*, vol. 20, no. 5, pp. 21–23, 2016, doi: 10.1108/14777280610688014.
- [24] E. Technologies, "SOMatic Viewer: Implementation of an Interactive Self-Organizing Map Visualization Toolset in Processing and Java," Master's thesis, 2013.
- [25] L. Yang, Z. Ouyang, and Y. A. Shi, "A Modified Clustering Method Based on Self-Organizing Maps and Its Applications," Procedia Comput. Sci., 2012.
- [26] H. Elghazel and K. Benabdeslem, "Different Aspects of Clustering the Self-Organizing Maps," Neural Process. Lett., 2014.
- [27] H. Elghazel and K. Benabdeslem, "Towards B-coloring of SOM," Lect. Notes Comput. Sci., vol. 2009, pp. 322-336, 2009.

- [28] J. Liu and L. Xu, "Improvement of SOM Classification Algorithm and Application Effect Analysis in Intrusion Detection," Adv. Intell. Syst. Comput., 2019.
- [29] A. S. Danielsen et al., "Self-Organizing Maps for Clustering Hyperspectral Images," Remote Sensing, vol. 13, no. 20, 2021.
- [30] E. Sabrina, "Klasifikasi Penyakit Diabetic Retinopathy Menggunakan Metode Learning Vector Quantization (LVQ)," *Jurnal Teknik Elektro*, vol. 6, no. 2, 2017.
- [31] L. Heryawan, "Deteksi Dini Retinopati Diabetik dengan Pengolahan Citra Berbasis Morfologi Matematika," *IJCCS (Indonesian Journal of Computing and Cybernetics Systems)*, vol. 11, no. 2, p. 209, 2017.

**Publisher's Note:** Publisher stays neutral with regard to jurisdictional claims in published maps and institutional affiliations.